Analysis of spacecraft materials discrimination using color indices for remote sensing for space situational awareness

Jacqueline A. Reyes[a,*], Heather M. Cowardin[b], Miguel Velez-Reyes [a]

[a] *University of Texas at El Paso, 500 W. University Ave., El Paso, TX, 79968, USA*

[b] *NASA Johnson Space Center, Orbital Debris Program Office, Houston, TX, 77058, USA*

ABSTRACT

The increasing number of space missions have resulted in an augmented density of artificial objects positioned in orbital domains near Earth. Knowing the material composition of the resident space object can be of value in object identification and risk assessment using remote sensing techniques. To perform this task, it is increasingly imperative to optically characterize spacecraft materials to identify unique material-specific spectroscopic markers. In this work, a variety of materials frequently utilized by the aerospace industry in spacecraft design and construction were analyzed using reflectance spectroscopy. The collected data provide a spectral characterization baseline for modern-day and historical spacecraft materials. The color index was computed for standard astronomical and suggested theoretical filter passbands and compared to each other in their capability to discriminate materials belonging to different classes. The color index was calculated from reflectance spectra of common spacecraft materials in their pristine, as-received conditions that fell under different family groupings. Different color-index combinations were studied using color-color diagrams. Visual and quantitative analysis of the color-color diagrams were used to evaluate the possibility of discriminating materials from one another by means of optical measurements. Results of the analysis show that polyimide and photovoltaic materials are most easy to discriminate from all other materials via color indices using different filter passbands evaluated in this study.

Keywords: spectral reflectance; spacecraft materials; optical characterization; color index; space situational awareness, remote sensing.

* Corresponding author e-mail: jareyes10@miners.utep.edu

1. INTRODUCTION

Space situational awareness (SSA) refers to knowledge of the space environment, including location and function of resident space objects (RSOs) that currently inhabit space domain. Although the location of objects populating the space domain is a significant aspect of SSA that can provide critical knowledge for the safety of any one resident space object (RSO), there are additional pieces of information that can be beneficial towards the overall intelligence that contributes to SSA. In addition, ascertaining material composition of RSOs, including orbital debris, provides insight for a more comprehensive understanding of objects populating space domain and the potential risk associated with high-speed objects of different material categories.

The evaluation of RSO material composition therefore provides key knowledge necessary to characterize an article. This information can be derived from the optical properties of materials in orbit using optical remote sensing. If space hardware materials can be distinguished from one another using optical measurements, then a taxonomy-based approach for material classification can help us characterize RSOs with greater effectiveness. This is possible since different classes of materials have unique optical properties.

Asteroids and planetary bodies have been evaluated remotely through the means of spectroscopic measurements [1, 2, 3, 4, 5]. Furthermore, spectroscopic measurements have been employed to study human-made materials [6, 7, 8, 9, 10, 11, 12], showing their efficacy for remote object characterization. RSO material composition information can also be obtained

with photometry using select astronomical filter systems. This optical measurement technique is employed to deduce optical characteristics of space objects by assigning a color index value with targets viewed through a telescope. This is made possible when using an optical filter possessing a defined passband to view desired targets. The various astronomical filter bandpass involved in a photometric measurement can then help determine material brightness (*i.e.*, magnitude) in each respective observed filter band to calculate a color index. The color index can then be assigned to objects with the aim of evaluating optical differences when compared to one another. The approach of using a color index to characterize spacecraft articles derived from photometric data has been established by Murtazonv, Nosova, Kupriyanov, and Prokof'eva [13] and confirmed by [14, 15, 16] amongst others. This photometric approach has been translated into characterizing materials in the laboratory setting for comparison to RSOs [7, 8]. Additional examples of these methods can be found in much of Cowardin's work [6].

In this work, reflectance spectroscopy was applied to measure the reflectance signatures for common spacecraft materials with the aim of calculating color indices using various passbands throughout the visible and near-infrared regions of the spectrum. Popular astronomical filter systems, such as those from the Sloan Digital Sky Survey, were used to evaluate material color index in addition to select infrared filters. In order to further support material distinguishability, new theoretical passbands were defined for use in the color index calculations. The motivation for this research is defined by the on-going need for the SSA community to characterize RSOs via ground-based measurements and laboratory data to better classify RSOs by material categories. It is sought to determine if this can be accomplished via discriminating against measurable color indices that can be acquired in a laboratory setting and applied to telescopic observations.

MATERIALS & METHODS

The primary objective for conducting this research is to evaluate material discrimination performance using color index values derived from the reflectance signature of a given material. The first goal executed to achieve this taxonomy approach for material discrimination included selecting a balanced set of materials that are commonly used in space applications that fell under the different material classes: metals, polymers, ceramics, and composites. Once these materials were chosen, their reflectance signatures were measured (350-2500 nm range, visible to short wave infrared), and were evaluated depending upon their absorption and reflectance features. The second goal encompassed conducting repeatability analysis and calculating various color indices for each of the selected materials using established and theoretical filter passbands within the 350-2500 nm wavelength range. This was performed to associate material brightness with color index value. The third goal was to perform visual pattern recognition for material discrimination via color index. Full details of all experiments are presented in [17]. The paper presents the noteworthy results.

2.1. Materials

For this study, it was important that the materials selected for spectral analysis represented various classifications of materials, including metals, polymers, ceramics, and composites, to evaluate any potential patterns that resulted from their optical measurements. The materials commonly incorporated in space design that were included in this study are listed in Table 1. Due to the nature of the materials used for this study, not all materials are the same size or shape. The materials studied in the laboratory were acquired with the same instrumentation set-up with a limited field-of-view of 25°. To characterize each material, multiple spectral measurements (with a minimum of 3 spectral measurements sampled) are collected on each material and averaged over the entire surface of each material to address any reflectance variations in the target of interest. For complex materials, a large number of spectral measurements may be required to fully characterize the material signature.

2.2. Spectral Measurements

Reflectance spectroscopy can be utilized during remote optical analysis for material characterization and optical size calculations from albedo. The technique involves measuring the light reflected off a material surface over a range of wavelengths to evaluate absorption/reflectance features in the acquired spectra. Results will depend on the properties of the material under examination. The spectral measurements conducted in this work were performed on materials in their pristine, as-received conditions.

Measurements took place in a laboratory environment within a dark room to optimize result accuracy and minimize any potential interference of scattered or stray light. Test configuration for measurement set-up involved the material specimen to be placed flat on a horizontal surface representing the origin of set-up. The illumination source and the spectroradiometer fiber optic feed were positioned approximately 45° to that of the specimen and directly opposite to each other. The spectroradiometer employed for this study was an Analytical Spectral Device (ASD) FieldSpec Pro spectrometer with range capability between 350-2500 nm. An ASD supplied tungsten-quartz-halogen lamp provides the illumination source for diffuse reflectance measurements. The ASD spectroradiometer measures the radiance reflected by the material specimen. A white standard (Spectralon ®) provides a high reflectance Lambertian surface with a near perfect flat reflective signature of 99% reflectance in the 350-2500 nm spectral range. The radiance reflected by each specimen is normalized by the radiance reflected by the white standard to obtain the calibrated absolute reflectance signature- presented as absolute reflectance. The standard deviation was calculated for all data sets and provided an indication of measurement accuracy.

Table 1. Materials included in spectral measurements for optical analysis.

Material Class	**Material Sample**			
Metal (alloy)	6061 aluminum alloy	7075 T6 aluminum alloy	Ti6Al4V	
Metal	Copper			
Polymer	Polyimide (Kapton®)	Kevlar®	Mylar®	Spectralon®
Polymer based	White Paint			
Composite (structure)	Silicon solar cell	Germanium solar cell		
Composite	Carbon Fiber Reinforced Polymer (CFRP)			
Polymer matrix composite	Circuit Board – Green	Circuit Board – Blue	Circuit Board – Brown	Circuit Board – Red
Ceramic matrix composite	Phenolic impregnated carbon ablator (PICA)			
Ceramic	Tile White	Fused Silica Glass	Ceramic foam	

2.3. Color Index

Because color index is dependent upon flux within a given passband, all combinations of index values for established astronomical filter system passbands and arbitrary passbands were applied to evaluate their potential for material discrimination. The established visible filters and their respective passbands that produced the best results in this study are listed in Table 2, and full details are presented in [17]. The subset of established infrared filters included in the analysis are used by United Kingdom Infra-Red Telescope (UKIRT), which cover the 836-1784 m, regime [18]. Lastly, the theoretical filters applied for this analysis are also listed in Table 2 for a modified visible passband (V1) and four infrared passbands (IR1, 3, 4, and 16), all of which have a strict 100 nm coverage.

Table 2. List of astronomical filters (established and theoretical) and passbands that provided worthy results in this study.

Filter (established)	**Passband λ Range (nm)**	**Filter System Source**	**Filter (theoretical)**	**Passband λ Range (nm)**
g	406-544	Sloan	V1	400-500
r	558-682	Sloan	IR1	800-900
i	705-835	Sloan	IR3	1000-1100
z	839-1094	Sloan	IR4	1100-1200
Z	836-929	UKIRT	IR16	2400-2500
Y	979-1081	UKIRT		
H	1492-1784	UKIRT		

In astronomical photometry applications [19], *magnitude* refers to 2.5 times the logarithm of the apparent brightness of an object over a passband in the electromagnetic spectrum. The *color index* represents the difference in magnitude between the two different filter passbands and is given by

$$f1' - f2' = -2.5[\log_{10}(I_{f1}) - \log_{10}(I_{f2})] = -2.5\log_{10}\left(\frac{I_{f1}}{I_{f2}}\right) \quad (1)$$

where $f1'$ and $f2'$ represent the magnitude at each passband, and I represents its brightness. In our experiments, the brightness is the integrated area under the material reflectance curve within the given filter passband.

Brightness (I) can be calculated from summing the area under the reflectance curve for the material measured between each incremental wavelength. The $Area$ under the curve between two wavelengths in the spectral signature is computed using the trapezoidal formula

$$Area_f = \left(\frac{(R_f + R_{f+1})}{2}\right) * (\lambda_{f+1} - \lambda_f) \quad (2)$$

where R represents the reflectance value of the measured material at a given wavelength (λ), and subscript f is used to indicate that each of the respective variables correspond to values within the passband of a given SDSS filter. The ASD spectral resolution (*i.e.* $\Delta = \lambda_{f+1} - \lambda_f$) is 3 nm in the VNIR and 10 nm in the SWIR. The brightness (I) of a material in the passband between $\lambda_1$and λ_2 is given by

$$I = \sum_{\lambda_1}^{\lambda_2} Area_f \quad (3)$$

where $\lambda_1$and λ_2 represent the wavelength at the onset and at the end of the filter's passband range respectively. Having calculated the brightness (I) for one filter, this method can be repeated for each different astronomical filter, and the magnitude can be compared between two filters ultimately using the color index formula (Equation 1). This work explored the use of classic and modern astronomical filter systems, as well as experimenting with proposed theoretical filter passbands for calculations to assess material discrimination using color indices for existing and potentially new filter systems.

2.4. Color-Color Diagrams and Distances between Indices

Visual analysis is performed on color-color diagrams, which is a scatter plot of one-color index against another index to further evaluate hot the reflectance of various materials may be better isolated for discrimination. This initial study is performed with humans-in-the-loop but provides a pathway for machine learning applications for pattern recognition and discrimination. For quantitative analysis, the Euclidean distance between point in the color-color diagram is used to quantify material separability. The equation for the Euclidean distance is given by

$$d_e((i,j),(h,k)) = \sqrt{(j-i)^2 + (k-h)^2} \quad (4)$$

where $(i,j),(h,k)$ represents the color index values of two points in the color-color diagram.

RESULTS & DISCUSSION

A total of 20 different samples of material often utilized in spacecraft design had their reflectance signature measured in the 350-2500 nm spectral range using the ASD spectroradiometer. The features observed from each of the reflectance signatures in this study can be used to help understand the physical appearance and chemical makeup of the measured materials with the intent of possibly discriminating between them optically according to their material classification. Significant features in VIS (350-700 nm), NIR (700-1300 nm), and SWIR (1300-2500 nm) that were present and likely

attributors in one or more of the analyzed materials are summarized in Table 3. The color-color diagrams relevant to demonstrating a sufficient degree of discrimination in certain materials measured are presented and quantitatively discussed.

Table 3. Absorption features present in the VIS/NIR/SWIR reflectance data for the selected material samples [20].

Wavelength (nm)	Feature	Cause(s)	Materials with Feature Attributed
350-700	High absorption	Black color	Silicon-based solar cell, germanium-based solar cell, carbon fiber reinforced polymer (CFRP)
350-700	Relatively high absorption	Brown color	Brown circuit board
400	Sharp increase in reflectance	Blue color	Blue circuit board
550	Increase in reflectance	Green color	Green circuit board
600	Sharp increase in reflectance	Gold color	Copper, polyimide (Kapton)
650	Sharp increase in reflectance	Red color	Red circuit board
850	Strong absorption dip	Aluminum content	Al 6061, Al 7075 T6
1400	Absorption dip	O-H	Circuit boards, Mylar, Kevlar, fused silica glass
1700	Asymmetric absorption doublet	O-H, first overtone	White paint, silicon-based solar cell
1900	Single absorption dip	C-O, O-H, second overtone	Circuit boards, copper, polyimide (Kapton) white tile
2180	Asymmetric absorption doublet	N-H, second overtone C-H, C-O, C=O stretches	Polyimide (Kapton), Mylar
2200	Broad absorption feature	C-H	Fused silica glass
2300	Prominent single absorption dip	C-H, N-H stretches	Circuit boards, Mylar, silicon-based solar cell
2450	Low intensity absorption dip	O-H	Circuit boards

3.1. Reflectance Signatures

The measured reflectance signatures for the materials selected in this study are presented in Figure 1. Note, any spectra that may have resulted in a computed reflectance greater than one is due to the nature of that material being highly specular, delivering a saturated reflectance response to the detector and simply being greater than the Lambertian response calibrated by the Spectralon®.

Additionally, though phenolic impregnated carbon ablator (PICA) and the printed circuit boards are technically considered composite materials, they are being analyzed as ceramics and polymers respectively due to the detector measuring characteristics of a material surface. PICA is a ceramic matrix composite, and the PCBs are polymer matrix composites. This indicates that the composite material introduced in the material system is embedded within the matrix, therefore making it worthy to analyze PICA as a ceramic and the circuit boards as polymers. Therefore, the materials analyzed as composites are related to composite structure in terms of their configuration. These included solar cells with either silicon or germanium substrate components, and carbon fiber reinforced polymer (CFRP), which although a polymer matrix composite, is comprised of fibers woven in a specific orientation to enhance properties and strengthen said material.

Within the metals category, it is significant to note the absorption features present at 850 nm, which can be used to discriminate aluminum-based metals from other metals. This is shown in Figure 1a where the two aluminum alloys have an absorption feature at 850 nm while the copper and titanium alloy do not. Copper can be isolated from other metals due to its characteristic red-orange optical hue, and this is represented by absorption at the onset of VIS with an increase in reflection near 600 nm. Other than color features in VIS and the aluminum absorption feature in NIR, the reflectance signatures for the metals were predominantly featureless in the IR. This behavior is typical of unpainted metals.

Polymeric materials are clearly different in reflectance response than materials belonging to other classifications due to the substantial amount of absorption features in the infrared region of the spectrum. From the polymers selected for measurement, there are multiple absorption features present at specific wavelengths that are shared between the various polymers (Figure 1b). For example, at 1900 nm, all polymers exhibit some level of absorption, though it is most prominently seen in the Kapton® Kevlar® (Kapton films and Kevlar fibers are manufactured by E.I. du Pont de Nemours and Co.), and white paint materials, and noted as a doublet from the Mylar® sample (Mylar is manufactured by Dupont Teijin Films from the resin polyethylene terephthalate). Absorption features that are specific to certain polymers can be seen, for example, by the Kevlar sample which demonstrated prominent absorption at ~1500 nm, whereas the other polymer samples were absent of this characteristic. Further, though all selected polymers exhibit some degree of absorption at ~1650 nm, it is apparent that Mylar exhibits the strongest absorption feature as this wavelength when compared with other polymers. The four printed circuit boards (PCB's) resulted in analogous absorption responses throughout the IR. The selected polymer materials for analysis also provided multiple spectral features in the VIS regime. The Kapton and red PCB samples show increased reflection at 650 nm, and white paint and Mylar samples resulted in high reflectance at the onset of VIS before 400 nm. The blue and green PCBs reflected in VIS at 450 nm and ~525 nm to coincide with their optical color property as well.

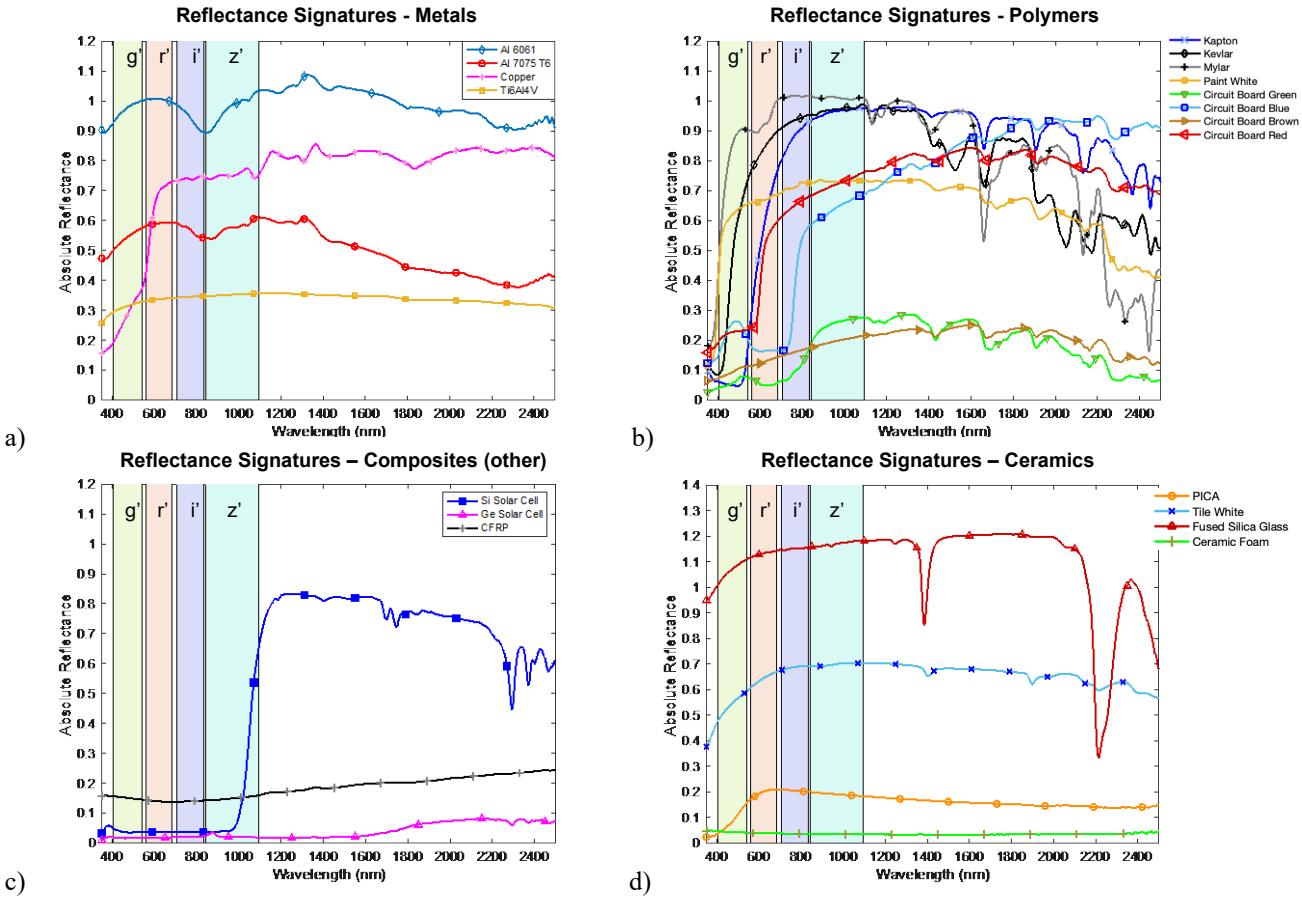

a) b) c) d)

Figure 1: Absolute reflectance spectra for various materials divided into a) metals, b) polymers, c) composite structure, and d) ceramics. Sloan *griz* passbands depicted within the 400-1100 nm regime.

The silicon-based solar cell responded as expected (Figure 1c), with high absorption throughout VIS and up to 1000 nm, followed by a sharp increase in reflection at 1000 nm, while demonstrating absorption features at 1700 nm and throughout the 2250-2500 nm range. The germanium-based solar cell also resulted in its typical reflectance response; producing extremely high absorption throughout the full 350-2500 nm range with a sole, small peak feature at 850 nm.

Lastly, the carbon fiber reinforced polymer (CFRP) composite maintained a relatively low reflectance with no additional features to note.

Analysis of the selected ceramics demonstrated similar optical behavior to metals due to the lack of numerous organic absorption features in the IR and maintaining relatively constant reflectance throughout the 350-2500 nm range (Figure 1d). However, the fused silica glass material sample exhibited only two strong absorption features present at 1400 nm and 2200 nm due to O-H and C-H bonds, respectively. There are weak spectral absorption features present for the white tile material at 1400, 1900, and 2200 nm, though not as evident as the strong organic feature presence in polymeric materials. The PICA and ceramic foam materials remained featureless throughout the full measurement range and exhibited much lower reflectance values relative to the other two ceramics measured.

3.2. Color-Color Diagrams

Color index values were calculated for traditional, modern, and theoretical filter passbands. Scatter plots of one-color index against another index were performed and analyzed visually and quantitatively. The materials that exhibited most frequent and/or effective discrimination between them and all other materials via color index were the silicon solar cell, the germanium solar cell, and the polyimide (Kapton). The color-color diagrams that produced best material discrimination results are presented next. The analysis details for the totality of color index pairs considered in this work are presented in [17].

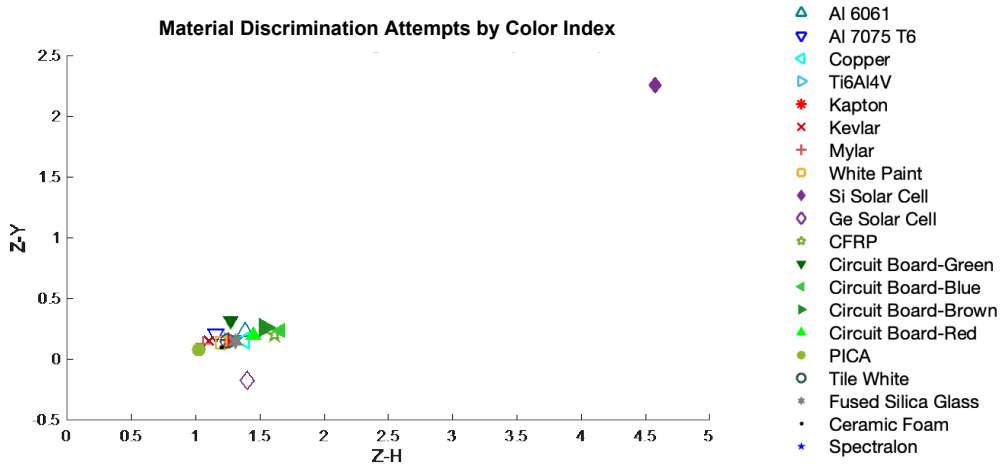

Figure 2: Color-color diagrams for Z-Y versus Z-H color indices according to their respective filter passbands.

The Z-Y versus Z-H color-color diagram (Figure 2) provided results that performed well in separating the silicon solar cell from all other materials. The diagram exhibits the clustering of all materials measured where the average Z-Y is 0.158 and the average Z-H is 1.304, with the exception of the silicon solar cell that has a Z-Y value of 2.42 and a Z-H value of 4.57. The distance between the silicon solar cell and the material nearest in color index (blue circuit board) resulted in a large value of 3.545.

The indices resulting from the V1-IR16 versus IR4-IR16 diagram provided effective discrimination of the germanium solar cell, amongst other interesting details to consider (Figure 3). The germanium solar cell had a V1-IR16 value of 1.59 and an IR4-IR16 value of 1.50 was separated by 1.236 from the blue circuit board (nearest in color index). Additionally, the green circuit board had a distance of 0.861 from Kevlar, which was the material closest to it. The silicon solar cell and Kapton materials delivered color index values that were near equal to each other in both IR4-IR16 and V1-IR16 indices, with a distance of 0.114 between these indices. They could be separated from other materials by having the largest V1-IR16 indices compared to all other materials, with Kapton resulting in 2.87 and the Si solar cell having a value of 2.97 for said index. The Mylar sample also describes some level of separation in regard to both indices, having a V1-IR16 value of -0.93 and an IR4-IR16 value of -1.18, and a distance of 0.802 between it and the white paint, its closest material in color index.

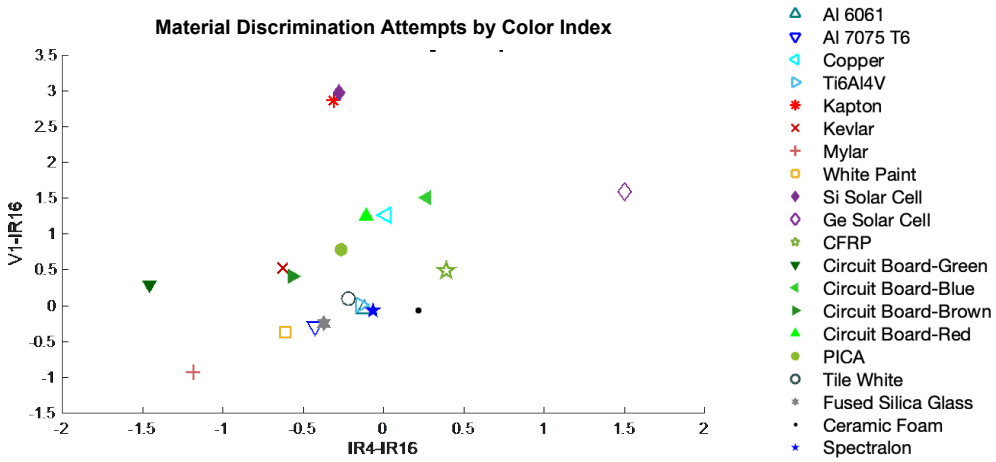

Figure 3: Color-color diagrams for V1-IR16 vs. IR4-IR16 color indices according to their respective filter passbands.

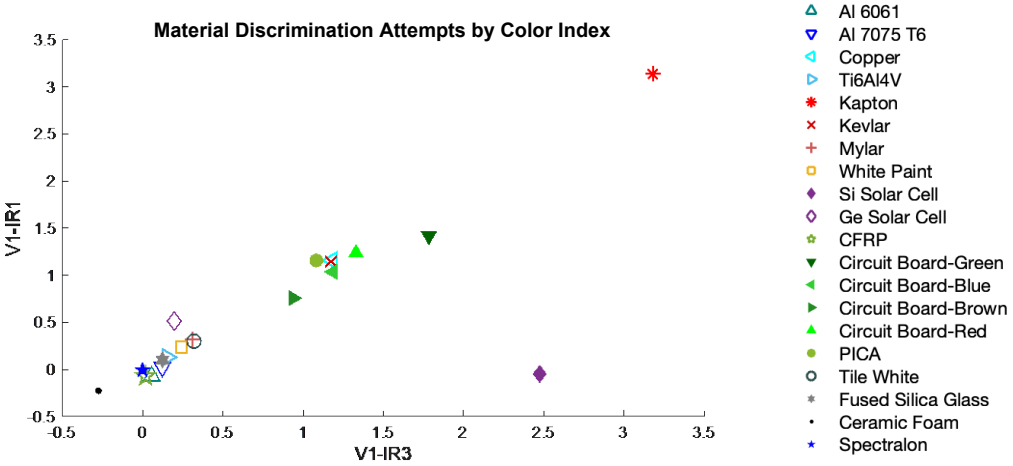

Figure 4: Color-color diagrams for V1-IR1 versus V1-IR3 color indices according to their respective filter passbands.

Additionally, it was found that the V1-IR1 versus V1-IR3 color-color diagram provided not only good repeatability in both indices but also the simultaneous discrimination of the polyimide (Kapton) and silicon solar cell materials (Figure 4). While the silicon solar cell was only isolated in the V1-IR3 regime, with a color index value of 2.47 and distance of 1.617 between it and the green circuit board, the polyimide (Kapton) sample was isolated for both indices with a V1-IR3 value of 3.18 and a V1-IR1 value of 3.14. Kapton also resulted in having a substantial distance value of 2.216 between it and the green circuit board, the material closest in index to it. In addition, this color-color diagram also resulted in values for both aluminum materials that were nearly equal, with a distance of 0.112 between their indices.

It can be noted that this color index, using these passbands, can be compared to the narrow passbands provided by established astronomical filter systems. Therefore, the *g'-z'* versus *g'*-Y color-color diagram was generated [17]. Through comparison, though similar to the V1-IR1 versus V1-IR3 diagram, it did not yield the same results in effectively isolating the silicon solar cell material while also not exhibiting the same degree of separation for the polyimide. For quantitative purposes, the distance between the silicon solar cell and its nearest neighboring material index (green circuit board) in the *g'-z'* versus *g'*-Y diagram resulted in 0.517, a value of 1.100 less than what was seen in the V1-IR1 versus V1-IR3 diagram. Furthermore, the polyimide material had a distance of 1.575 between it and the silicon solar cell for the *g'-z'* versus *g'*-Y diagram, while the distance value between it and the green circuit board resulted in 2.216 for the V1-IR1 versus V1-IR3 diagram, a difference of 0.614 between these nearest neighbor material index distance results.

3.2. Relating Color Indices and Spectral Signatures

For a better visualization of how this color index data is derived from the material spectral signatures, the reflectivity curves for the silicon solar cell, germanium solar cell, and polyimide (Kapton) are plotted with the carbon fiber reinforced polymer (CFRP) reflective signature superimposed to better compare the color index outcomes of these signatures (Figure 5). The silicon solar cell demonstrated the most discrimination from other materials when using classic filters to calculate their color indices as seen from the Z-Y versus Z-H color-color diagram (Figure 2). It is therefore seen that there are large variations in flux for the silicon solar cell, where the area under the reflectivity curve is evidently much less within the Z passband versus the Y and H passbands, though the flux is relatively the same between all three passbands (Z, Y, and H) for the CFRP material.

For the germanium solar cell, the largest distance between it and the material closest to it on the color-color diagrams studied was seen in the V1-IR16 versus IR4-IR16 diagram, which made use of variable/theoretical passbands for calculating material color indices. Again, this can be seen in Figure 5b, where the germanium-based solar cell demonstrated differences in flux between the three depicted passbands, leading to its unique color index value and discrimination from other materials in the respective color-color diagram.

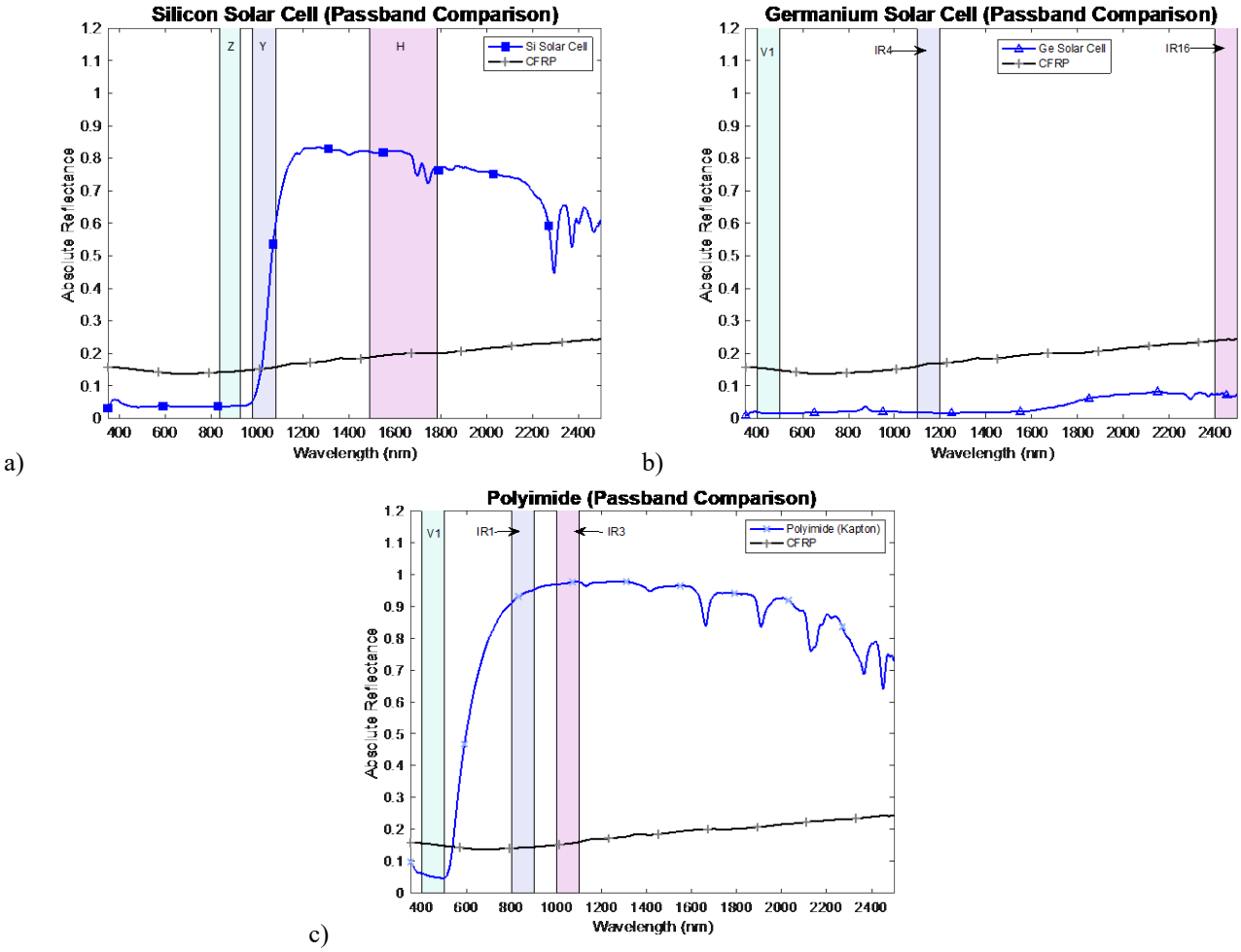

Figure 5: Reflectivity curves for a) silicon solar cell material, with Z, Y, and H filter passbands depicted within the graph, b) germanium solar cell sample with V1, IR4 and IR16 passbands depicted within the graph, and c) polyimide (Kapton) sample with the V1, IR1 and IR3 passbands depicted within the graph, and CFRP material signature for comparison.

Finally, the polyimide (Kapton) exhibited most isolation in the V1-IR1 versus V1-IR3 color-color diagram (Figure 4), where variable/theoretical passbands were used to calculate indices. The V1, IR1, and IR3 passbands are depicted on the Figure 5c spectral plot along with reflectivity curves for the polyimide and CFRP materials. This figure shows the stark differences in flux between the V1 and the IR1 and IR3 proposed passbands for the Kapton sample, where the area under the curve is much smaller within the VI passband versus the IR1 and IR3 passbands. Compared to the CFRP material, which has a relatively flat spectra between the 350-2500 nm range, and therefore showed fewer differences between the three aforementioned passbands, the polyimide had larger variation between these passbands and therefore exhibited greater discrimination in color index for the V1-IR1 versus V1-IR3 diagram.

Of the color-color diagrams using modern filter passbands for color index, the *r'-i'* versus *g'-i'* diagram demonstrated greatest distance between Kapton and the material closest to it, with a distance value of 1.678. However, the *i'-z'* versus *g'-i'* diagram was almost as effective in isolating the polyimide with a distance value of 1.676 between it and its nearest neighboring material in index. The data results for this and details regarding other color-color diagram results explored can be found in [17] for the interested reader.

4. CONCLUSION

It has been well established throughout literature and studies that optical measurements serve as a valuable means to aid remote object classification through analysis of their spectral features. Remote observations using filter systems make use of assigning objects by color index. From the multitude of astronomical filter measuring systems available, certain filters with specific passbands can be intentionally selected to better discriminate specific materials or material clusters. These measuring tools can provide enhanced data when utilizing passband combinations that fall in regions throughout both, the visible and infrared regions of the spectrum. Though location and magnitude of absorption/reflectance features within material spectra can be used for obvious discrimination of materials possessing organics within their chemistry versus those without, it was explored how these characteristics can translate into color index value for an alternate method of using optical measurements to characterize materials.

The comparison of uses for classic, modern, and theoretical filter passbands to calculate material color indices were evaluated. Through comparisons, conclusions drawn suggest greater effectivity in discriminating the germanium solar cell and polyimide materials using the proposed theoretical passbands. The silicon solar cell material, however, still demonstrated better discrimination/separation from other materials via color-color diagrams using the established astronomical Z, Y, and H filter passbands.

Because the taxonomy approach conducted in this work was an initial step toward assessing the ability to better categorize materials using laboratory-based data, there is much work that can be carried out in the future to advance strategies involved in material characterization for increased space situational awareness. For example, this study focused on the spectra of individual materials, however hyperspectral imagery can be employed to deduce material composition from an unresolved object with a mixed measured spectra [21].

In addition, spectral libraries may consider having the capability to generate color-color diagrams for observational purposes. In doing so, collecting material measurements at various phase angle and rotation configurations would provide a comprehensive, data-driven/machine learning model for remote observations. If spectral libraries can generate color indices autonomously from their spectral input, this can offer some degree of guidance for color associated with common spacecraft materials. In turn, this can help bridge the gap between laboratory-based measurements and remote observations. The aim to better characterize RSOs via remote observations with supporting data from laboratory analyses in hopes to better refining the uncertainty with RSO's based on the optical signatures provided.

5. ACKNOWLEDGEMENTS

The authors would like to acknowledge NASA Johnson Space Center's Orbital Debris Program Office for providing required capabilities for performing reflectance spectroscopic measurements in optimal conditions. Jacqueline A. Reyes acknowledges individuals Daniel P. Engelhart, Ryan C. Hoffmann, Elena Plis, Vanessa Murray, and Dale C. Ferguson, who are associated with the Air Force Research Labs, for their mentorship and color index calculation resources. Jacqueline A. Reyes would like to recognize and thank the NASA Fellowship Activity program

(Award #80NSSC18K1702) that has supported her research and academic studies at the University of Texas at El Paso. Dr. Velez-Reyes acknowledges support by the Office of the US Assistant Secretary of Defense for Research and Engineering through the Research and Education Program for Historically Black Colleges and Universities and Minority-Serving Institutions (HBCU/MI) under Award No. W911NF-19-1-0011. Opinions, interpretations, conclusions, and recommendations are those of the authors and are not necessarily endorsed by the Department of Defense or NASA. On behalf of all authors, the corresponding author states that there is no conflict of interest.

6. REFERENCES

[1] K. Markus, L. Moroz, G. Arnold, et al., "Reflectance spectra of synthetic Fe-free ortho- and clinoenstatites in the UV/VIS/ IR and implications for remote sensing detection of Fe-free pyroxenes on planetary surfaces," *Planetary and Space Science,* 2018.

[2] A. Pisello, F. P. Vetere, M. Bisolfati, et al., "Retrieving magma composition from TIR spectra: implications for terrestrial planets investigations," *Nature Scientific Reports,* 2019.

[3] E. A. Cloutis, V. B. Pietrasz, C. Kiddell, et al., "Spectral reflectance “deconstruction”of the Murchison CM2 carbonaceous chondrite and implications for spectroscopic investigations of dark asteroids," *Icarus,* 2018.

[4] K. Kitazato, R. E. Milliken, T. Iwata, et al., "The surface composition of asteroid 162173 Ryugu from Hayabusa2 near-infrared spectroscopy," *Science,* 2019.

[5] O. Poch, I. Istiqomah, E. Quirico, et al., "Ammonium salts are a reservoir of nitrogen on a cometary nucleus and possibly on some asteroids," *Science 367,* 2020.

[6] H. M. Cowardin, "Characterization of Orbital Debris over Optical Wavelengths via Laboratory Measurements," University of Houston, Houston, TX, 2010.

[7] P. Seitzer, S. M. Lederer, H. Cowardin, et al., "Visible Light Spectroscopy of GEO Debris," in *Advanced Maui Optical and Space Surveillance Technologies Conference (AMOS)*, Maui, Hawaii, 2012.

[8] K. Jorgensen, "Using Reflectance Spectroscopy to Determine Material Type of Orbital Debris," University of Colorado at Boulder, Boulder, CO, 2000.

[9] K. Abercromby, P. Abell and E. Barker, "Reflectance Spectra Comparison of Orbital Debris, Intact Spacecraft, and Intact Rocket Bodies in the GEO Regime," in *Proceedings of the Fifth European Conference on Space Debris*, Darmstadt, Germany, 2009.

[10] D. Bedard and G. A. Wade, "Time-resolved visible/near-infrared spectrometric observations of the Galaxy 11 geostationary satellite," *Advances in Space Research,* 2016.

[11] A. Vananti, T. Schildknecht and H. Krag, "Reflectance Spectroscopy Characterization of Space Debris," *Advances in Space Research,* 2017.

[12] K. Jorgensen, J. Africano, K. Hamada, et al., "Physical properties of orbital debris from spectroscopic observations," *Advances in Space Research ,* pp. 1021-1025, 2004.

[13] P. P. Sukhov and K. P. Sukhov, "On Some Problems of Photometric Identification of Geostationary Satellites," *Kinematics and Physics of Celestial Bodies,* vol. 31, no. 6, pp. 314-318, 2015.

[14] J. M. Sorvari, "Photometry of Artificial Satellites Application to the Ground Electro-optical Deep Space Surveillance (GEODSS) Program," Defense Technical Information Center, 1979.

[15] A. Murtazov, "Physical simulation of space objects’ spectral characteristics for solving the reverse problem of their photometry," *American Journal of Modern Physics,* vol. II, no. 6, pp. 282-286, 2013.

[16] E. C. Pearce, H. A. Ford, T. Schildknecht, et al., "Rapid Characterization of Geosynchronous Space Debris with 5-color Near-IR Photometry," in *Proceedings of the Advanced Maui Optical and Space Surveillance (AMOS) Technologies Conference*, Maui, Hawaii, 2017.

[17] J. A. Reyes, "Reflectance Spectral Characterization and Taxonomy Applications of Spacecraft Materials to Aid Space Situational Awareness," The University of Texas at El Paso, El Paso, 2022.

[18] A. Lawrence, S. Warren, O. Almaini, et al., "The UKIRT Infrared Deep Sky Survey (UKIDSS)," *Monthly Notices of the Royal Astonomical Society,* vol. 379, no. 4, 2007.

[19] T. E. o. E. Britannica, ""colour index"," Encyclopedia Britannica, 16 September 2008. [Online]. Available: https://www.britannica.com/science/color-index-astronomy. [Accessed 19 August 2022].

[20] J. A. Reyes and H. Cowardin, "Spectral characterization of spacecraft materials used in hypervelocity impact testing," in *SPIE Algorithms, Technologies, and Applications for Multispectral and Hyperspectral Imaging XXVII*, 2021.

[21] J. Yi and M. Velez-Reyes, "Simplified simulation of unresolved objects in hyperspectral remote sensing for space situational awareness," in *Proc. SPIE 11392, Algorithms, Technologies, and Applications for Multispectral and Hyperspectral Imagery XXVI*, 2020.

[22] P.-E. Danielsson, "Euclidean Distance Mapping," *Computer Graphics and Image Processing,* vol. 14, no. 3, pp. 227-248, 1980.